Journal of the European Ceramic Society 22 (2002) 653–660

www.elsevier.com/locate/jeurceramsoc

Synthesis and characterization of nano-$LiMn_2O_4$ powder by tartaric acid gel process

Y.M. Hon, S.P. Lin, K.Z. Fung*, M.H. Hon

Department of Materials Science and Engineering, National Cheng Kung University, Tainan 70101, Taiwan

Received 16 February 2001; received in revised form 25 May 2001; accepted 3 June 2001

Abstract

Polycrystalline nano-$LiMn_2O_4$ spinel powder was synthesized by the tartaric acid gel process and developed without any detectable minor phase at 300 °C. The powders synthesized by the tartaric acid gel process had a relatively smaller particle size, larger specific surface area and narrower particle size distribution than those prepared by the conventional solid state reaction. The average valence of manganese decreased with increasing synthesis temperature and resulted in an increase of the lattice parameter with calcination temperatures. As temperatures were increased to above 500 °C, $LiMn_2O_4$ underwent phase transition from a cubic to a tetragonal phase by removing oxygen ion in the lattice. From the results of MAS NMR, $LiMn_2O_4$ spinels formed at 300–800 °C had a large Knight shift of ~520 and 560 ppm in reference to LiC1.

Keywords: Batteries; Cathode; $LiMn_2O_4$; Lithium–ion battery; Nano-powder; Powders-chemical preparation; Tartaric acid

1. Introduction

The spinel $LiMn_2O_4$ is a very promising cathodic material with economical and environmental advantages as compared with layered compounds such as $LiCoO_2$ and $LiNiO_2$.[1] From the point of view of starting materials, price and toxicity, the $LiMn_2O_4$ spinel has a considerable advantage.

Obviously, the preparation of spinel $LiMn_2O_4$ phase by solid-state reactions involves the raw materials of manganese oxides, nitrate or carbonate with lithium hydroxide, nitrate or carbonate at temperatures reacting at as high as 700–900 °C, and the final product usually contains the impurity phases, irregular morphology, larger particle size, and broader particle size distribution.[2,3] In general, as for the batteries application, it is believed that single-phase, homogeneity, uniform particle morphology with submicron size distribution, and large surface area are considered as desired characters in order to achieve better electrode properties.

Therefore, several techniques, such as sol-gel,[4] co-precipitation,[5] melt-impregnation,[6] the citric acid gel method,[7,8] the tartaric acid gel method[9,10] and Pechini process[11] have been developed. On conventional solid state reaction, solid reactants are simply heated at high temperatures for an extended period until minor phases disappear. On many occasions, intermittent grindings and mixings are involved to remove the diffusion barrier, which could lace the product with inadvertent impurities. A better way to avoid this situation would be by keeping the composition of the reactants as homogeneous as possible. In the tartaric acid gel process, the chemical reaction takes place in an atomic/molecular scale and long-range diffusion is not required. Therefore, products can be formed at much lower temperatures.

In this work, a tartaric acid method was developed to synthesize nano-$LiMn_2O_4$ powder directly from lithium acetate and manganese acetate. Without using other chemicals (such as glycol, ammonium hydroxide, ammonium chloride or polyhydric alcohol) and additional processing steps, this synthesis method was considered to be inexpensive and simple. The effect of calcination temperature on phase transition, specific surface area, crystal size and average valence of manganese for $LiMn_2O_4$ powders has been studied.

* Corresponding author. Tel./fax: +886-6-2380208.
E-mail address: kzfung@mail.ncku.edu.tw (K.Z. Fung).

0955-2219/02/$ - see front matter
PII: S0955-2219(01)00382-X

2. Experimental

2.1. Precursors formed by the tartaric acid gel process

$LiMn_2O_4$ powders were prepared by the tartaric acid gel process. Lithium acetate (98% purity, Aldrich) and manganese acetate (99% purity, Showa Chemicals Inc.) used as sources for lithium and manganese were dissolved in ethanol, the molar ratio of metal ions Li^+: Mn^{2+} being controlled at 1 to 2. The metal–ion ethanol solution was then mixed with the ethanol solution of tartaric acid (99.5% purity, Katayama). During mixing, the solution abruptly transformed into a viscous gel. The final gel contained 0.025 M Li^+, 0.05 M Mn^{2+} and 0.1 M tartaric acid. The gel was subsequently heated in an oven at 68 °C to remove the ethanol. After drying, the lithium manganese tartrate precursor became hard agglomerates with pinkish color.

2.2. Calcination process

The precursor was then heated at 200 °C for 6 h to slowly remove the moisture. Subsequently the calcination process was conducted at temperatures ranging from 265 to 800 °C for 24 h in air. Finally, the calcined powders were furnace-cooled to room temperature for further investigation.

2.3. Thermal and structure analysis

Thermal analysis was carried out using differential scanning calorimeter (DSC, Netzsch 404) and thermogravimetric analysis (TG, TA2950) to investigate the possible phase transformation between 25 and 600 °C with a heating rate of 1, 5, 10 and 15 °C/min, respectively.

The phase identity, crystal structure, and lattice constants of the materials were investigated using Rigaku X-ray diffractometer (XRD) with the CuK_α radiation at 30 kV, 20 mA. The XRD data were collected between 10 and 70° of 2θ angles with a step interval of 0.01 and a scanning rate of 1°/min. Lattice constants were determined by a least-squares refinement of the d-spacing, which were measured in comparison with an internal standard of pure Si.

2.4. Chemical analysis

The concentrations of lithium and manganese in the samples calcined at various temperatures were analyzed by inductively coupled plasma (ICP, Janell-Ash, ICAP 9000). The average valence of manganese was determined by the titration method. About 0.06 g of the sample was dissolved in 20 ml of an acidified 0.08 M Fe(II) solution. During dissolution, the higher Mn oxidation states (III) and (IV) were reduced to Mn(II) by the oxidation of Fe(II) to Fe(III). The excess Fe(II) was back titrated with 0.018 M $KMnO_4$.

2.5. FT–IR and NMR analysis

Fourier transform infrared spectrometer (FT–IR, JASCO FT/IR-410) was used to study the structure coordination of the precursors. Each sample was mixed with KBr and examined at the wavenumber range from 400 to 4000 cm^{-1}.

Solid-state ^7Li NMR spectra were obtained using a Bruker AVANCE 400 spectrometer. ^7Li spectra were acquired at 155.5 MHz, using spinecho method, recycling delay of 1 s and 90° pulse width for ^7Li was 3.3 μs. All spectra were referenced to an external $LiCl_{(aq)}$ standard and acquired with spinning speeds of 15 kHz.

2.6. TEM analysis

Pieces of the cathode were ultrasonically de-agglomerated and dispersed on an amorphous carbon film supported by a Cu grid for TEM observation. A Jeol JEM-3010 operated at 200 kV accelerating voltage and equipped with a double-tilt holder was used for imaging and electron diffraction.

3. Results and discussion

3.1. Thermal analysis

Fig. 1 shows the DSC/TG curves for the lithium manganese tartrate precursors at the heating rates of 1, 5, 10 and 15 °C/min, respectively. In our previous study,[12] tartaric acid had no weight loss below 200 °C. However, the lithium manganese tartrate precursor has about 30% weight loss below 200 °C that may be attributed to the removement of water and acetate group.

There is a sharp exothermal peak at 303 °C for the samples heated with a rate of 1 °C/min. The temperature corresponding to this sharp exothermal reaction increased and split into two broad peaks as the heating rate was increased. Combining the results of TG and DSC, it is found that a large amount of weight loss accompanies the exothermal reaction at a lower temperature. No apparent weight loss is found in the exothermal reaction at a higher temperature. It is believed that the exothermal peak of DSC at a lower temperature was due to the combustion of an organic component in the sample. Another exothermal peak observed at a higher temperature was caused by the formation of $LiMn_2O_4$ spinel. In the tartaric acid gel process, the tartaric acid does not only function as a chelating agent but can also release a large amount of heat when the oxidation of organic compounds takes place violently. Such an energy release can easily stimulate the synthesis of lithium manganese oxide. In principle, the combustion of organic materials occurred first and then the

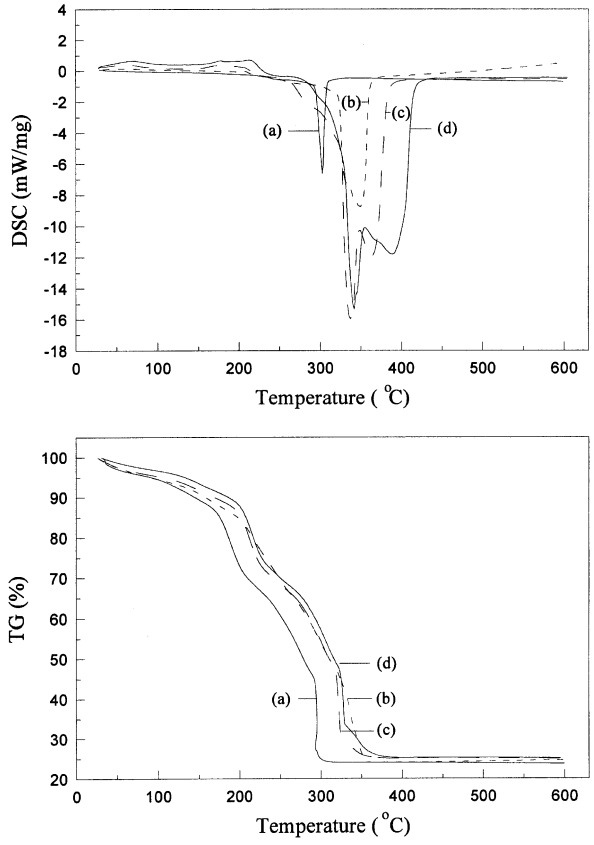

Fig. 1. DSC/TG analysis for lithium manganese tartrate precursors at heating rates of (a) 1 °C/min, (b) 5 °C/min, (c) 10 °C/min, (d) 15 °C / min in air.

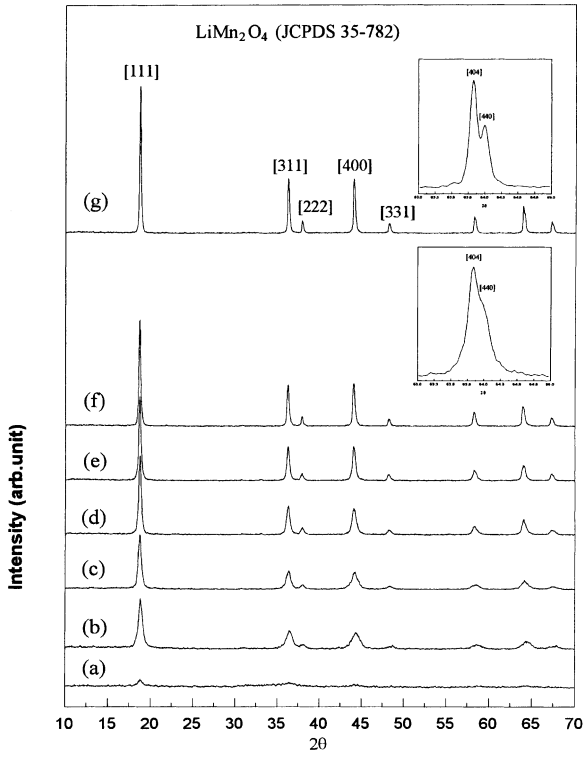

Fig. 2. XRD patterns of (a) precursor and $LiMn_2O_4$ powders calcined at (a) 265 °C, (b) 300 °C, (c) 400 °C (d) 500 °C, (e) 600 °C, (f) 700 °C, (g) 800 °C for 24 h.

lithium manganese oxide formed. This phenomenon is more distinguishable at a high heating rate.

Thus, when the precursor was heated at a higher rate as shown in Fig. 1(d), the first reaction did not occur until 340 °C. This temperature is higher than that using a lower heating rate. The reason can be just inhomogeneous heating at high heating rate which causes the temperature of the precursor to be lower than what was measured. Such a behavior is fairly common in a fast-heating process. For the formation of lithium manganese oxide, it is expected that the energy barrier is considerably higher than the oxidation of the organic precursor because the reaction involved the rearrangement of cations and oxygen ions. At low heating rates (e.g. 1 °C/min), the time periods from the beginning to the end of reactions is several times longer than that for high heating rate (e.g. 15 °C/mm). That is the reason why the separated exothermic peaks were not observed at low temperatures.

3.2. Characterization of $LiMn_2O_4$ powders

3.2.1. Structure analysis and phase transition

The XRD patterns of lithium manganese tartrate precursor and calcined at various temperatures for 24 h in air are shown in Fig. 2. The lithium manganese tartrate precursor is amorphous and started to transform into crystalline spinel $LiMn_2O_4$ powder at 300 °C in air. The impurities such as Li_2CO_3, MnO_2 or Mn_2O_3 were not observed. Apparently, the lithium manganese tartrate precursor transformed into spinel $LiMn_2O_4$ without any formation of minor or metastable phase in the calcination temperature ranges. These results strongly suggest that this tartaric acid gel method was much superior to the solid-state reaction since pure spinel $LiMn_2O_4$ powders can be prepared at a much lower calcination temperature due to the shorter Li–Mn ion distance and atomic-scale metal ion distribution in the precursor.

The [440] peak of the cubic $LiMn_2O_4$ phase splitted into the [440] and [404] peaks of the tetragonal phase as the calcination temperature increased. The similarities in the X-ray patterns of samples between cubic and tetragonal phases show that the tetragonal phase had the slightly distorted spinel structure. It is believed that the cubic to tetragonal transformation took place due to the small amount of oxygen loss from the lattice on the particle surface when the precursor was calcined at a high temperature.[13] In Yamada[14] and Sugiyama's[15] studies, the oxygen deficiency was found as a function of oxygen pressure and temperature and determined that the cubic to tetragonal transformation took place at 835.5 °C which was higher than that observed in this study. The

difference in particle size should be the main reason to cause the variation in transition temperatures. In their work, $LiMn_2O_4$ was synthesized by solid-state reaction technique that usually produced powder in the micron range.

However, $LiMn_2O_4$ fabricated using tartaric acid gel process gave powder in the nanometer range with large specific surface area. The finer particles provided shorter diffusion distance as well as much greater surface area for fast kinetics during the chemical reaction. Thus, the cubic to tetragonal transformation of lithium–manganese-oxide prepared by tartaric acid gel process can take place at much lower temperatures.

Fig. 3 shows the effect of calcination temperature on lattice constant, a and average valence of manganese in $LiMn_2O_4$ powders. It is seen from the figure that the lattice constant increased from 8.1569 to 8.2290 Å when increaseing the calcination temperatures from 300 to 800 °C. However, the average valence of manganese decreased with a calcination temperature increase. Hence, the formation of a more oxidized manganese ion was observed at a lower temperature because manganese ions were stable preferentially as Mn^{4+} at a lower temperature.[16] Thus, the lattice constant of the spinel $LiMn_2O_4$ calcined at lower temperatures shows a smaller value than that of the spinel $LiMn_2O_4$ calcined at higher temperatures.

The reduction of symmetry from cubic to tetragonal indicates a change in local symmetry of MnO_6 octahedron from O_h to D_{4h} resulting from a cooperative Jahn–Teller distortion of Mn^{3+} ions in octahedral sites.[17] The results indicate that the reduction of Mn^{4+} to Mn^{3+} in cubic spinel tended to distort the lattice and formed the tetragonal lattice. Therefore, the oxygen content in the surrounding atmosphere is expected to play an important role in the stability of the cubic spinel.[13] In the present work, the loss of oxygen in the $LiMn_2O_{4-\delta}$ also increased the concentration of Mn^{3+}.

3.2.2. Specific surface area, crystal size and morphology

Fig. 4 shows the effects of calcination temperature on the specific surface area and crystal size of $LiMn_2O_4$ powders. It can be seen that the specific surface area decreased abruptly at the calcination temperatures between 300–400 °C. This result is attributed to the large amount of heat release from the combustion of the precursor at about 350 °C, which caused the agglomeration of fine particles. At temperatures above 400 °C, the specific surface area of powders decreased gradually. The crystal size is seen to increase from 21.1 to 75.5 nm as the calcination temperatures increased from 300 to 800 °C.

Fig. 5 shows the bright field images and selected area diffraction (SAD) of TEM for $LiMn_2O_4$ powders calcined at 300 and 500 °C, respectively. It is observed that for the particle size of powder calcined at 300 °C in the range of 15–25 nm and the electron diffraction results show a well-ordered single $LiMn_2O_4$ phase. As the calcination temperature increased, the particles of the powder grew apparently and the crystallinity of phase increased.

3.3. FT–IR and NMR studies of $LiMn_2O_4$

The FT–IR spectra of spinel $LiMn_2O_4$ calcined from lithium manganese tartrate precursor at various temperatures were shown in Fig. 6. The spectra of $LiMn_2O_4$ calcined at 400 °C show two bands at 516 and 616 cm^{-1}. For samples calcined at high temperature, the two bands in the spectra shifted to higher frequencies. For example, the sample calcined at 800 °C shows two

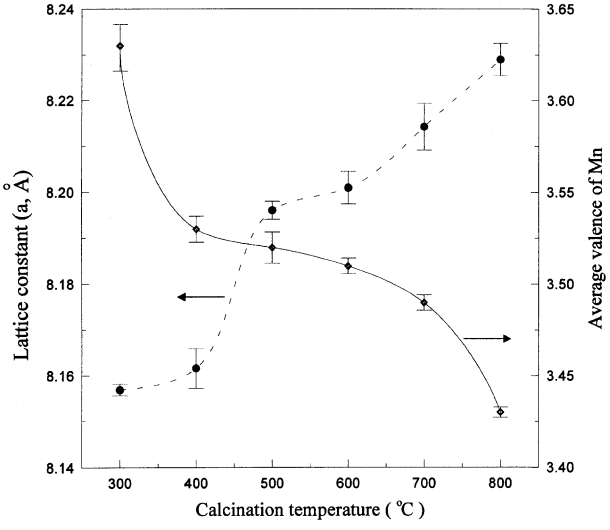

Fig. 3. Effects of calcination temperature on lattice constant and average valence of manganese of $LiMn_2O_4$ powders.

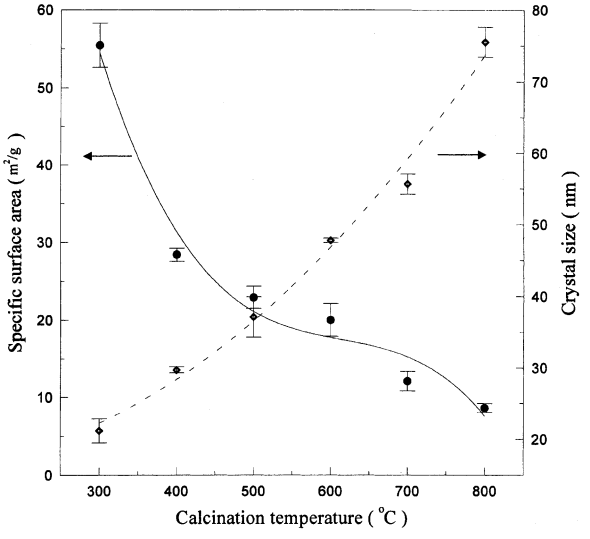

Fig. 4. Effects of calcination temperature on specific surface area and crystal size of $LiMn_2O_4$ powders.

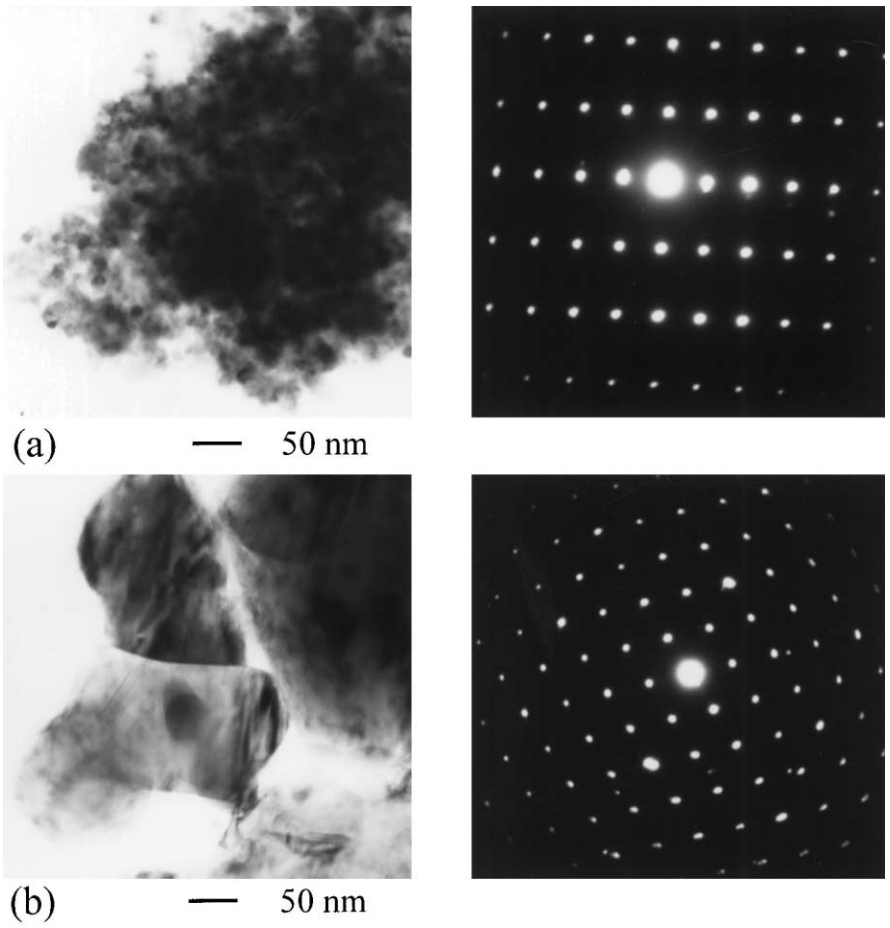

Fig. 5. TEM images of bright field and selected diffraction area (SAD) for $LiMn_2O_4$ calcined at (a) 300 °C, (b) 500 °C for 24 h.

bands at 526 and 626 cm^{-1}. The high frequency bands of the FT–IR spectra located at ~516 and 616 cm^{-1} are attributed to the asymmetric streching modes of the MnO_6 group.[18,19] The bands of OH (3432 and 1630 cm^{-1}) still are clearly observed in Fig. 6(a) and (b). Thus, the organic complex was not completely removed but still remained at a temperature lower than 400 °C.

The ^7Li MAS–NMR spectra of several spinels were acquired with spinning speeds of 15 kHz as shown in Fig. 7. The spectra for samples calcined from 300 to 800 °C are considered as two spinning side bands, The Knight shifts of spinel calcined at 300 and 800 °C are situated around ~523, 568 ppm, and ~525, 560 ppm, respectively, which indicate that the full width at half maximum (FWHM) of NMR spectra decreased with calcination temperature. The ^7Li MAS–NMR spectra obtained is different compared to the previously published results.[20] In spectra of the samples synthesized from Li_2CO_3 and Mn_2O_3 by solid-state reaction at 550 °C, four broad resonances were observed at 498, 546, 575 and 630 ppm by Lee.[21] As the synthesis temperature was raised to 850 °C, only one resonance at 520 ppm was observed which indicates the lithium ion occupiing at 8a position. Nitta[22] reported that the MAS

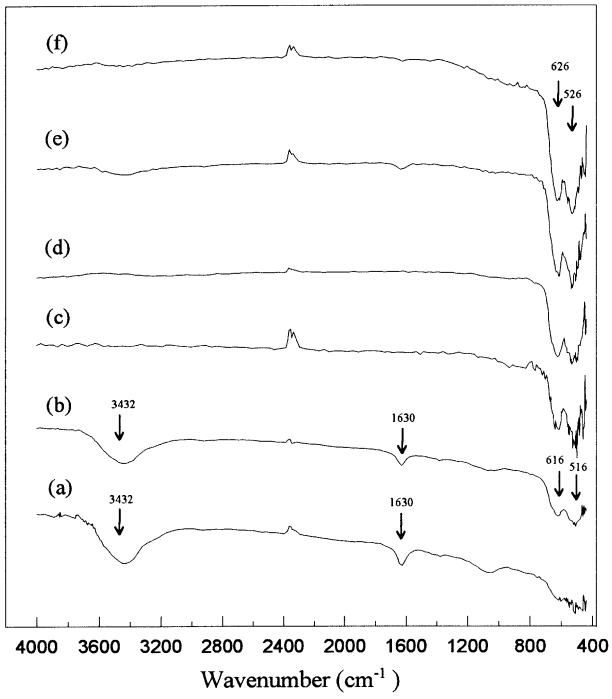

Fig. 6. FT–IR of $LiMn_2O_4$ calcined at (a) 300 °C, (b), 400 °C, (c) 500 °C (d), 600 °C, (e) 700 °C, (f) 800 °C for 24 h.

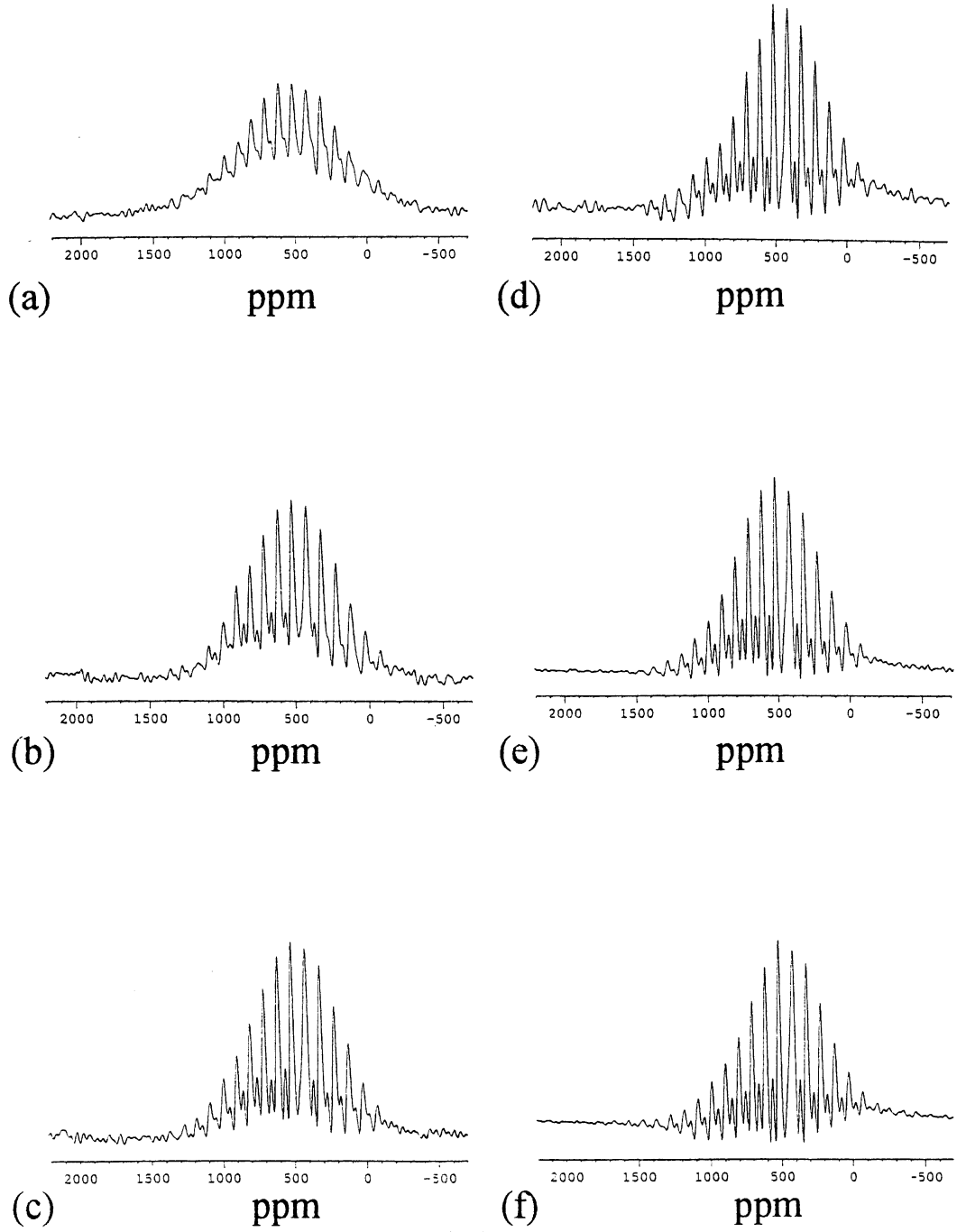

Fig. 7. ^{7}Li MAS NMR spectra of $LiMn_2O_4$ spinels calcined at (a) 300 °C, (b) 400 °C, (c) 500 °C, (d) 600 °C, (e) 700 °C, (f) 800 °C with spinning speeds of 15 kHz.

^{7}Li–NMR spectra of lithium manganese oxide synthesized from MnO_2 and Li_2CO_3 at 350 °C (LT–$LiMn_2O_4$) had a broad signal with the peak at 762 ppm. The spectra of the lithium manganese oxide synthesized at 700–900 °C (HT–$LiMn_2O_4$) had a broad signal with the peak at about 600 ppm, where chemical shift appeared a lower frequency shift than that of LT–Mn_2O_4. In our result, the two spin side bands did not apparently shift with the calcination temperature but the intensity increased with increasing calcination temperature.

It is generally known that the $LiMn_2O_4$ is spinel-structured (space group Fd3m) as a cubic close-packed array of oxygen in the 32e position. Half of the octahedral interstices, at the 16d position, are occupied by the manganese ions, forming a three-dimensional framework of edge-sharing [MnO_6] octahedra. Lithium ions

occupy one-eighth of the tetrahedral interstices, at the 8a position. Each 8a tetrahedron shares common faces with four neighboring empty octahedra at the 16c position which, together with 48f tetrahedra, forms a three-dimensional network of interstitial space. The energies for a lithium interstial at the unoccupied tetrahedral and octahedral interstices in λ–MnO_2 have been calculated by Ammundsen et al.[20] Lithium occupation for the 16c octahedral sites in λ–MnO_2 is less favorable than that of the 8a by 1.1 eV. The 48F and 8b tetrahedral sites are energetically unfavorable for the Li^+ ion as they share two and four faces with Mn 16d octahedra, respectively. In consideration of the influence on these lithium sites at different distances from manganese with high paramagnetism, for example, 8a and 16c positions, the 16c site, which is located in closer to the manganese, is more influenced by high paramagnetism and the chemical shift appears at a higher frequency shift. The 8a site is not so much influenced by high paramagnetism and the chemical shift appears at a lower frequency shift. In our ^{7}Li MAS–NMR spectra, the chemical shift at $\sim$520 ppm is conformed to the lithium ion occupation at 8a position. The chemical shift at $\sim$560 ppm does not fit to lithium ion occupation at other positions, such as 16c or 16d, or at 8a site in other lithium manganese oxide compounds, for example: $Li_4Mn_5O_{12}$ or $Li_2Mn_4O_9$.[21] It is believed that the chemical shift at $\sim$560 ppm indicates the lithium ion still occuping at 8a position in $LiMn_2O_4$ but having different distances to neighboring manganese and oxide ions.

4. Conclusion

It was seen that as the calcination temperature increased, the lattice constant increased whereas the average valence of manganese decreased. The nano-$LiMn_2O_4$ powder was calcined at 300 °C exhibits small crystal size of 21 nm and large specific surface area of 55.5 m^2/g. The FT–IR spectra for $LiMn_2O_4$ calcined at 400 °C show two bands at 516 and 616 cm^{-1} that are attributed to the asymmetric streching modes of MnO_6 group. As calcine temperature increasing, two bands in the spectra shifted to higher frequencies. From the result of MAS NMR, the Knight shifts of spinel calcined at 300 and 800 °C are situated around $\sim$523, 568 ppm, and $\sim$525, 560 ppm, respectively that indicated the lithium ion occupies at 8a position but has two different distances to neighboring manganese and oxide ions.

Acknowledgements

This work was financially supported by the National Science Council of Taiwan, Grant No. NSC 89-2216-E-006-052, which is gratefully acknowledged.

References

1. Guyomard, D. and Tarascon, J. M., Li metal-free rechargeable $LiMn_2O_4$ carbon cells: their understanding and optimization. *J. Electrochem. Soc*., 1992, **139**(4), 937–948.
2. Gao, Y. and Dahn, J. R., Synthesis and characterization of $Li_{1+x}Mn_{2-x}O_4$ for Li–ion battery applications. *J. Electrochem. Soc*., 1996, **143**(1), 100–114.
3. Endres, P., Fuchs, B., Sack, S. K., Brandt, K., Becker, G. F. and Praas, H. W., Influence of processing on the Li:Mn ratio in spinel phases of the system $Li_{1+x}Mn_{2-x}O_{4-\delta}$. *Solid State Ionics*, 1996, **89**, 221–231.
4. Passerini, S., Coustier, F., Giorgetti, M. and Smyrl, W. H., Li–Mn–O aerogels. *Electrochemical and Solid-State Letters*, 1999, **2**(10), 483–485.
5. Naghash, A. R. and Lee, J. Y., Preparation of spinel lithium manganese oxide by aqueous co-precipitation. *J. Power Sources*, 2000, **85**, 284–293.
6. Xia, Y., Takeshige, H., Noguchi, H. and Yoshio, M., Studies on a Li–Mn–O spinel system (obtained by melt-impregnation) as a cathode for 4 V lithium batteries. Part 1. Synthesis and electrochemical behaviour of $Li_xMn_2O_4$. *J. Power Sources*, 1995, **56**, 61–67.
7. Yang, W., Liu, Q., Qiu, W., Lu, S. and Yang, L., A citric acid method to prepare $LiMn_2O_4$ for lithium–ion batteries. *Solid State Ionics*, 1999, **121**, 79–84.
8. Hon, Y. M., Fung, K. Z. and Hon, M. H., Synthesis and characterization of $Li_{1+\delta}Mn_{2-\delta}O_4$ powders prepared by citric acid gel process. *J. Eur. Ceram. Soc*., 2001, **21**, 515–522.
9. Tsumura, T., Shimizu, A. and Inagaki, M., Synthesis of $LiMn_2O_4$ spinel via tartrates. *J. Power Sources*, 1997, **3**(9), 593–599.
10. Pyun, S. I., Choi, Y. M. and Jeng, I. D., Effect of the lithium content on electrochemical lithium intercalation into amorphous and crystalline powdered $Li_{1+\delta}Mn_2O_4$ electrodes prepared by sol-gel method. *J. Power Sources*, 1997, **68**, 593–599.
11. Liu, W., Farrington, G. C., Chaput, F. and Dunn, B., Synthesis and electrochemical studies of spinel phase $LiMn_2O_4$ cathode materials prepared by Pechini process. *J. Electrochem. Soc*., 1996, **143**(3), 879–884.
12. Hon, Y. M., Chung, H. Y., Fung, K. Z. and Hon, M. H., NMR and FT–IR investigation of spinel $LiMn_2O_4$ cathode prepared by tartaric acid gel process. *J. Solid State Chem*., in press.
13. Hon, Y. M., Fung, K. Z. and Hon, M. H., Effect of temperature and atmosphere on phase stability and morphology of $LiMn_2O_4$ powder synthesized by citric acid gel process. *J. Ceram. Soc. Jpn*., 2000, **108**(2), 462–468.
14. Yamada, A. and Tanaka, M., Jahn–Teller structural phase transition around 280 K in $LiMn_2O_4$. *Mater. Res. Bull*., 1995, **30**(6), 715–721.
15. Sugiyama, J., Atsumi, T., Hioki, T., Noda, S. and Kamegashira, N., Oxygen nonstoichiometry of spinel $LiMn_2O_{4-\delta}$. *J. Alloys and Compounds*, 1996, **235**, 163–169.
16. Sun, Y. K., Lee, K. H., Moon, S. I. and Oh, I. H., Effect of crystallinity on the electrochemical behaviour of spinel $Li_{1.03}Mn_2O_4$ cathode materials. *Solid State Ionics*, 1998, **112**, 237–243.
17. Tarascon, J. M., Mckinnon, W. R., Coowar, F., Bowmer, T. N., Amatucci, G. and Guyomard, D., Synthesis conditions and oxygen stoichiometry effect on Li insertion into the spinel $LiMn_2O_4$. *J. Electrochem. Soc*., 1994, **141**(6), 1421–1431.
18. Barboux, P., Tarascon, J. M. and Shokoohi, F. K., The use of acetates as precursor for the low-temperature synthesis of $LiMn_2O_4$ and $LiCoO_2$ intercalation compounds. *J. Solid State Chemistry*, 1991, **94**, 185–196.
19. Pasquier, A. D., Orsini, F., Gozdz, A. S. and Tarascon, J. M., Electrochemical behavior of $LiMn_2O_4$–PPy composite cathodes in the 4-V region. *J. Power Sources*, 1999, **81–82**, 607–611.

20. Ammundsen, B., Roziere, J. and Islam, M. S., Atomistic simulation studies of lithium and proton insertion in spinel lithium manganates. *J. Phys. Chem. B*, 1997, **101**, 8156–8263.
21. Lee, Y. J., Wang, F. and Grey, C. P., ^{6}Li and ^{7}Li MAS NMR studies of lithium manganese cathode materials. *J. Am. Chem. Soc.*, 1998, **120**, 12601–12613.
22. Nitta, Y., Okamura, K., Nagayama, M. and Ohta, A., Lithium manganese oxides for rechargeable lithium batteries. *J. Power Sources*, 1997, **68**, 166–172.